

Scaling laws for large magneto-optical traps

This article has been downloaded from IOPscience. Please scroll down to see the full text article.

2010 Phys. Scr. 81 025301

(<http://iopscience.iop.org/1402-4896/81/2/025301>)

[The Table of Contents](#) and [more related content](#) is available

Download details:

IP Address: 193.48.228.28

The article was downloaded on 09/03/2010 at 15:26

Please note that [terms and conditions apply](#).

Scaling laws for large magneto-optical traps

G L Gattobigio^{1,2}, T Pohl³, G Labeyrie¹ and R Kaiser¹

¹ Institut Non Linéaire de Nice, UMR 6618 CNRS and Université de Nice Sophia-Antipolis, 1361 route des Lucioles, 06560 Valbonne, France

² Dipartimento di Fisica dell'Università di Ferrara and INFN-Sezione di Ferrara, 44100 Ferrara, Italy

³ Max Planck Institute for the Physics of Complex Systems, Nöthnitzer Strasse 38, 01187 Dresden, Germany

E-mail: Robin.Kaiser@inln.cnrs.fr

Received 7 May 2009

Accepted for publication 11 January 2010

Published 2 February 2010

Online at stacks.iop.org/PhysScr/81/025301

Abstract

Multiple scattering of light has been the main limitation of the maximum atomic density achievable in magneto-optical traps (MOTs). We present a detailed experimental investigation of the size and density scaling laws for large MOTs with up to $N = 10^{10}$ atoms, larger than those usually studied in detail. Most of our observations can be explained with previous models and only a few regimes show unexplained deviations. We also propose a new repulsion mechanism, based on the rescattered repumper photons that might limit the atomic density of atoms when the optical thickness for repumper light becomes important, adding an additional ingredient in the complexity of large MOTs.

PACS numbers: 32.80.Pj, 39.25.+k, 42.50.Vk

(Some figures in this article are in colour only in the electronic version.)

1. Introduction

Since the first realization of laser cooling and trapping of dilute atomic vapors, one important goal has always been the realization of a degenerate atomic gas, such as the Bose–Einstein condensate (BEC). Beyond the realization of BEC, large densities of cold atoms are also important for a variety of fundamental studies such as cold collisions and cold molecule formation, cold Rydberg atom experiments, photon localization, local field corrections for the index of refraction and coupled dipole–dipole experiments with cold atoms, with its potential impact for quantum computing.

Achieving high spatial densities has, hence, been as important as designing suitable cooling mechanisms [1, 2]. Very soon, it was realized that for a large number of atoms rescattering of the trapping light results in an effective repulsion force between the atoms [3, 4]. The spatial densities achievable in standard magneto-optical traps (MOTs) have thus been limited to about $n \approx 10^{10}–10^{11} \text{ cm}^{-3}$, and increasing the number of atoms N in such a MOT results in a MOT size (L) scaling as $L \propto N^{1/3}$, which corresponds to a constant density $n \sim N/L^3$. These density-limiting effects have been

studied by many groups [4–11], and several attempts have been made to circumvent this limitation, notably the so-called dark spontaneous-force optical trap (dark SPOT) [12]. A number of systematic studies have investigated the limits of such a dark SPOT, where the fraction p of atoms in the ‘bright’ hyperfine level (coupled to the cooling and trapping lasers) is an important parameter [12, 13]. Different mechanisms have been put forward to explain the observed limitation of the density $n(p)$, such as finite temperature effects, multiple scattering forces and cold collisions. For very large MOTs, the confining force might also become nonlinear (anharmonicity of the trap), which in extreme regimes is at the origin of self-sustained oscillations of the MOT [14].

In our setup we realize a large number of atoms $N \approx 10^{10}$, beyond the typical range used in most previous studies. In this paper, we present a systematic study of the sizes and densities in such a large MOT and show that the size of the MOT scales differently with the atom number N , depending on the method used to change the atom number. In section 2, we describe in detail our experimental setup and detection techniques. In sections 3 and 4 we compare and analyze the experimental data obtained using two different techniques to

vary the number of trapped atoms N : by varying either the *diameter* of the repumper laser (section 3) or its *intensity* (section 4). We finally discuss in section 5 results that cannot be explained by the standard models used for describing the scaling laws of a MOT. We also propose in this section a new model that takes into account an additional repulsion force.

2. Experimental setup and detection techniques

We prepare our atomic sample by loading a MOT from a dilute vapor of rubidium atoms. The experimental setup used for the present studies has already been described in [15], and we thus only briefly recall some features of our experimental setup, including calibration techniques.

A magnetic field gradient of typically 10 G/cm^{-1} is generated using a pair of coils along the O_z -axis. We use a master/slave configuration with subsequent amplification in a tapered amplifier for the MOT beam close to the $F = 3 \rightarrow F' = 4$ transition of the D2 line of ^{85}Rb (figure 1). We routinely obtain 180 mW power after spatial filtering, split into six beams with a waist of $w = 2.4 \text{ cm}$, directed in pairwise counter-propagation into a 10 cm sized cubic vacuum chamber. The repumper laser, close to the $F = 2 \rightarrow F' = 3$ transition of the D2 line of ^{85}Rb , is a master/slave configuration as well and is used in a retroreflection geometry along one direction only. The repumper beam diameter is expanded to $\Phi \approx 5 \text{ cm}$ using a telescope. A diaphragm placed at the conjugate position of the MOT allows one to vary the repumper diameter, thus modifying the effective capture volume of the MOT without directly affecting its dynamics. Indeed, there is no change of external MOT parameters (incident intensities, detunings, magnetic field gradient) when the atom number is changed using the repumper size. Alternatively, we can vary the intensity of the repumper laser (at fixed size), which also allows one to change the number of trapped atoms. However, in this case, we expect the overall dynamics of the MOT to be affected. We thus have two methods to change the number of trapped atoms and, as we will see, these methods lead to different MOT scaling laws.

The time sequence implemented in this study is a sequence of a MOT period of 30 ms followed by a ‘dark’ period of 5 ms. During the dark period, we switch off all beams and the magnetic field, leaving the atoms in free fall expansion for 2 ms before applying one or more probe beams. The ‘dark’ period is sufficiently short, such that we do not need to load new atoms to fill up the MOT. This is an important point, allowing a fast duty cycle and efficient data taking. As a probe we use either a single (weak) beam or the six trap beams of the cooling and trapping laser, with an adapted detuning. The single probe beam is used to measure the optical thickness $b(\delta)$ of the cloud, which depends on the detuning δ between the laser frequency ω_L and the atomic resonance frequency ω_{at} . In a different measurement, we use the six trap beams to illuminate the whole cloud and take images of the density distribution. A cooled CCD is used to record these fluorescence images. As we are interested in the sizes along all three dimensions of the MOT, we have directed two orthogonal images (labeled I_d and I_g) of the cloud onto the same CCD. From these images, we can retrieve spatially resolved information as well as the total fluorescence.

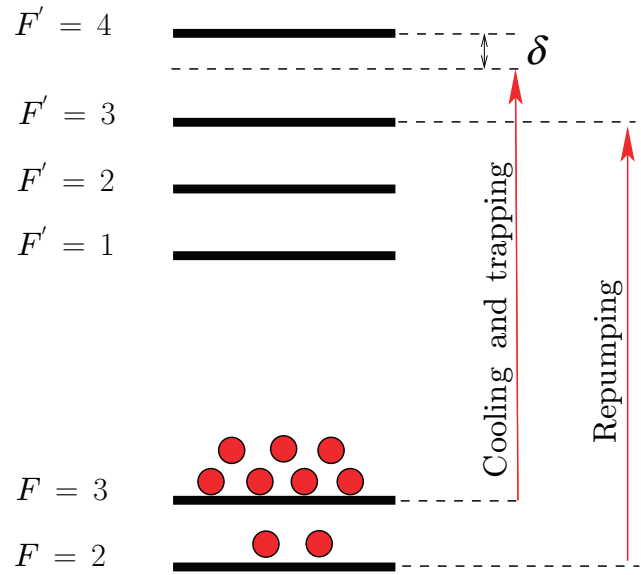


Figure 1. Relevant atomic hyperfine level of ^{85}Rb . The cooling and trapping laser is detuned by δ from the $F = 3 \rightarrow F' = 4$ transition. The repumper laser is tuned on resonance to the $F = 2 \rightarrow F' = 3$ transition.

A chopper, closed during the MOT period and opened during the dark period, prevents the strong fluorescence of the MOT from reaching the CCD. In this way, only the fluorescence induced by the off-resonance beams (typically at $\delta = -6\Gamma$) is recorded on the CCD. The use of such a large detuning to illuminate the cloud ensures that multiple scattering, which can modify the intensity distribution in the images, is negligible. Indeed, even the largest on-resonance optical thickness ($b_{\text{res}} \approx 40$) obtained in our experiments is reduced to a very small value at the imaging detuning:

$$b(\delta = -6\Gamma) = \frac{b_{\text{res}}}{1 + 4(\delta/\Gamma)^2} < 0.3, \quad (1)$$

where $\Gamma = 2\pi \cdot 6 \text{ MHz}$ is the inverse lifetime of the excited state. We have verified (see appendix (7.1)) that the size extracted via this procedure is independent of the detuning for $|\delta/\Gamma| > 5$. Hence, the CCD images provide us with fluorescence integrated along one line of sight, e.g. Oz :

$$I(x, y) = \eta \frac{\sigma_{\text{res}}}{1 + 4\delta^2/\Gamma^2} \int n(x, y, z) dz, \quad (2)$$

where η takes into account the detection efficiency of our imaging system, the intensity of the laser beams and the duration of the illumination. The expression of the on-resonance scattering cross-section σ_{res} will be given later.

In order to determine the total number of atoms, we measure the optical thickness of our atomic cloud along Oz by scanning a probe beam across the resonance and looking at the transmission $T(\delta)$ of this probe. This measurement is again done with the MOT switched off. For large enough optical thicknesses $b_{\text{res}} \gg 1$, the full-width at half-maximum Δ of the transmission curve $T(\delta)$ is connected to b_{res} by

$$b_{\text{res}} \approx \ln(2)[1 + (\Delta/\Gamma)^2]. \quad (3)$$

This technique allows one to measure in a reliable fashion large optical thicknesses, which is not possible by measuring

directly $T(\delta = 0)$ due to finite signal-to-noise ratio and probe laser spectral width. The measured b_{res} is proportional to the atomic density n integrated along the line of sight:

$$b_{\text{res}} = \sigma_{\text{res}} \int n(x = 0, y = 0, z) dz. \quad (4)$$

By comparing the value at the center of the image (2) and (4), we calibrate the detection efficiency of our imaging system. The total number of atoms N , assuming a Gaussian density profile (with rms sizes $\sigma_x, \sigma_y, \sigma_z$ along each dimension), is

$$N = (2\pi)^{3/2} \sigma_x \sigma_y \sigma_z n_0, \quad (5)$$

where n_0 is the peak atomic density. This can also be written as

$$N = \frac{(2\pi) \sigma_x \sigma_y b_{\text{res}}}{\sigma_{\text{res}}}. \quad (6)$$

Thus, combining the data from fluorescence imaging (σ_x, σ_y , see equation (2)) and the optical thickness measurement (b_{res}), we obtain the number of atoms N . This, however, requires the knowledge of the scattering cross-section:

$$\sigma_{\text{res}} = g \frac{3\lambda^2}{2\pi}, \quad (7)$$

where g is the effective coupling strength taking into account the Zeeman structure of the ground state [16]. We assume that the atoms are equally distributed among all the Zeeman sublevels of the ground state, which yields for our $F = 3 \rightarrow F' = 4$ transition $g = (2F' + 1)/3(2F + 1) = 3/7$. Using the second fluorescence image to obtain σ_z , we then have access to the maximum atomic density:

$$n_0 = \frac{b_{\text{res}}}{\sqrt{2\pi} \sigma_{\text{res}} \sigma_z}. \quad (8)$$

As discussed before, we extract from the two orthogonal images the rms sizes $\sigma_x, \sigma_y, \sigma_z$ of the atomic cloud along the three spatial dimensions. We have verified that the size along each direction obeys the same scaling laws. Thus, in the following, we will simplify the discussion by considering only an averaged size L , defined as

$$L = \frac{1}{3}(\sigma_x + \sigma_y + \sigma_z). \quad (9)$$

It is also possible to monitor the fluorescence by collecting the scattered light on a photodetector. This yields a strong signal during the long (30 ms) MOT sequence, with a complicated relation between scattered light and total number of atoms. However, during the short probe time, used to analyze our cold atomic sample when the MOT is switched off, a large detuning of the laser beams eliminates multiple scattering so that the fluorescence is then directly proportional to the atom number. The repumper laser can be switched off at the same time as the main MOT lasers or with a small positive or negative delay (see appendix 7.2), which influences the hyperfine populations during probing. As we will see below, this allows us to discriminate between the total number of atoms (sum of both hyperfine populations) and the number of atoms in the bright hyperfine level. When not otherwise mentioned, we switched off the repumper after the MOT laser and thus measured the total number of atoms during the short probe pulse.

After this detailed description of our experimental setup and protocol, we will now describe first qualitative observations followed by detailed studies of our MOT.

3. Repumper size-controlled atom number: $N(\Phi)$

3.1. Wieman model and nonlinear effects

In the past, one of our major objectives has been to optimize the optical thickness of our cloud. Hence, it seems reasonable to trap as many atoms as possible. It is also known, since the pioneering work of [3], that when more than 10^5 atoms are trapped the MOT size is determined by an interplay between the confining forces of the MOT beams and repulsive forces induced by multiple scattering of light. In the limit of moderate optical thickness (at the frequency used for trapping and cooling), the model put forward in [3] predicts a uniform density n in this regime. Denoting N as the total number of atoms and L (equation (9)) the size of the MOT, the uniform density regime implies that the trap size L scales as

$$L(N) \propto N^{1/3}. \quad (10)$$

In the following, we will call this the ‘Wieman model’.

The density limitation predicted by the Wieman model [3] can be understood in simple terms as a competition between a confining force F_{tr} and an effective repulsion force F_{ms} due to multiple scattering. These forces can be generally written as

$$F_{\text{tr}} = -\kappa r, \quad (11)$$

$$F_{\text{ms}} = G_3 n(r) r, \quad (12)$$

where κ is the spring constant of the trap and G_3 accounts for the competition between the shadow effect [17] and the repulsion due to the reabsorption of the MOT photons. A stationary density $n(r)$ requires a vanishing total force at any distance r , which yields a constant density of

$$n(r) = n_{\text{W}} = \frac{\kappa}{G_3}, \quad (13)$$

and leads to the $L(N) \propto N^{1/3}$ scaling law found in [3].

The model proposed in [3] was verified up to a certain number of trapped atoms $N \approx 5 \times 10^7$, above which a deviation was reported by the authors. They invoked higher order multiple scattering and trap nonlinearities as possible candidates to explain this behavior. Our goal has thus been to check the prediction of the Wieman model in the limit of a very large number of atoms $N > 10^8$.

In order to work out the influence of magnetic field gradients and nonlinearities in the MOT forces, we have developed a numerical treatment including such effects [18, 19]. In spirit, our model is similar to the Wieman model, i.e. we seek a self-consistent solution of the force balance equation

$$\mathbf{F}_{\text{tr}}(\rho, \mathbf{r}) + \mathbf{F}_{\text{ms}}(\rho, \mathbf{r}) = 0 \quad (14)$$

for the atomic density ρ , where \mathbf{F}_{tr} and \mathbf{F}_{ms} denote, respectively, the external trapping force and the interaction-induced force. As in the Wieman model, we perform a three-dimensional calculation but simplify the considerations by assuming a spherically symmetric intensity pattern and restrict ourselves to Doppler cooling and trapping mechanisms.

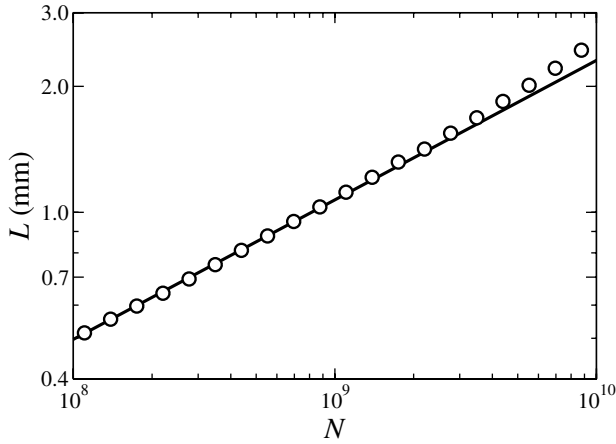


Figure 2. Calculated MOT size versus atom number (circles) compared to the $N \sim L^{1/3}$ power law (solid line). The MOT parameters are those of table 1.

Due to attenuation of light inside the atomic cloud, the intensities vary with position, such that the trapping force \mathbf{F}_{tr} carries an implicit dependence on the density profile $\rho(r)$.

The Wieman model assumes a homogeneous (spatially independent), i.e. Coulomb-like, interaction between the atoms. As mentioned above, this model predicts a constant density profile, with radius $L \propto N^{1/3}$. To obtain this simple solution, additional simplifications, such as a linear expansion of the external trapping force and a linear laser attenuation, are necessary. While these assumptions are well justified for small MOT sizes, they become questionable for large MOTs, as produced in our experiments. In general, the laser intensities and the absorption/reabsorption cross-sections depend on position and on the entire density profile due to the inhomogeneous Zeeman shift and the attenuation of laser light, respectively. We expect both of these effects as well as nonlinearities of the MOT potential to become increasingly important for large atom clouds.

Due to the nonlinear and nonlocal character of the full set of equations, finding direct numerical solutions for the atomic density is very demanding. Instead, we use an efficient test-particle method, which yields fast convergence to the physically relevant density profile and avoids difficulties with unstable solutions. As discussed in [18], this method also permits studies of the dynamical MOT behavior as described by the corresponding time-dependent kinetic equation for the atomic cloud.

While our numerical results for the size scaling apparently coincide with the prediction of the more simple Wieman model (see figure 2), the obtained density profiles, shown in figure 3, reveal dramatic differences. In contrast to the Wieman model, which predicts a constant density profile, our simulations yield a series of truncated Gaussian densities with changing atom number. While the width of the Gaussian density remains constant, the cut-off radius increases with increasing atom number, which results in the observed size scaling. This behavior can be understood by the fact that the effective repulsion is not homogeneous. In analogy to nonneutral plasmas, this would correspond to a space-dependent charge. A simple model predicts a constant charge density. As the repulsion becomes larger

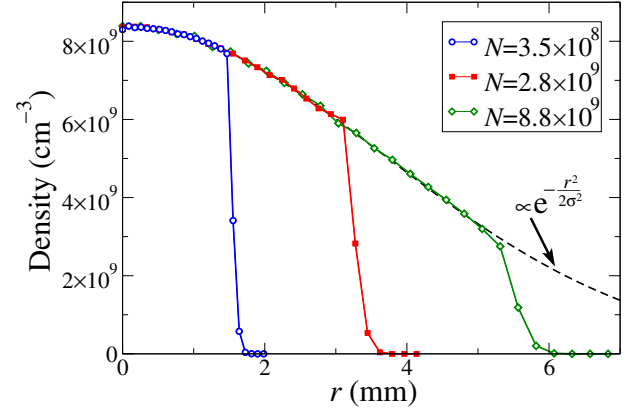


Figure 3. Calculated density profiles (color online) for three different atom numbers as indicated in the figure. The dashed line shows that the densities follow truncated Gaussian distribution, with $\sigma = 3.5$ mm. The MOT parameters are those of table 1.

Table 1. Standard MOT parameters as used in this paper.

MOT detuning	$\delta_{\text{MOT}} = -2.5\Gamma$
MOT intensity per beam	$I_{\text{MOT}} \approx 1.2 \text{ mW cm}^{-2}$
MOT beam waist	$w_{\text{MOT}} \approx 2.4 \text{ cm}$
Repumper detuning	$\delta_{\text{rep}} = 0$
Repumper intensity per beam	$I_{\text{rep}} \approx 0.5 \text{ mW cm}^{-2}$
Repumper beam diameter	$L_{\text{rep}} \approx 5 \text{ cm FWHM}$
Magnetic field gradient	$\nabla B = 10 \text{ G cm}^{-1}$

further away from the trap center, where the Zeeman shift tunes atoms closer into resonance, one can thus understand at least qualitatively that the atom number density is reduced at the border of the cloud.

Figures 2 and 3 exemplify the results of our calculations for the parameters of table 1. As shown in figure 2, the calculated atom number dependence of MOT size reveals the observed power law $N \sim L^{1/3}$, in accord with the Wieman model prediction (see equation (13)). At large N , we find slight deviations from the power-law behavior, heralding the onset of self-sustained oscillations at $N \sim 10^{10}$, above which the stationary solution disappears due to the onset of a dynamical instability [14, 18, 19]. A precise comparison with the experimental profiles is somehow difficult. Indeed, one needs to take into account the three-dimensional character of the experiment and thus use an Abel protocol [20] to extract a more reliable radial density profile. The experimental profile often has sharper edges than a pure Gaussian, but more systematic data analysis would be required in order to compare the experiment with the results shown in figure 3. Despite these finer details, the Wieman model apparently yields a surprisingly good description of size scaling even at large atom numbers.

3.2. Experimental results on $N(\Phi_{\text{rep}})$

3.2.1. Atom number versus repumper size: $N(\Phi_{\text{rep}})$. The number of trapped atoms loaded from background vapor is known to dramatically increase with size (Φ) of the MOT beams [6]. Indeed, the capture velocity (v_{capt}) of the MOT and the capture volume (V_{trap}) influence the number N of atoms as

$$N \propto v_{\text{capt}}^4 V_{\text{trap}}^{2/3}. \quad (15)$$

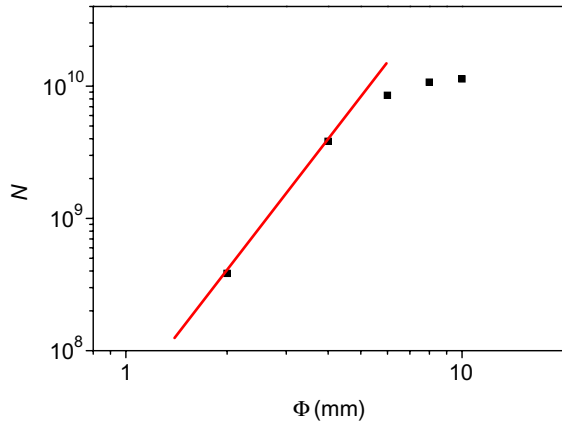


Figure 4. Number of trapped atoms as a function of diameter of the repumper laser. The solid line (red online) gives a power-law fit $N \propto \Phi^\nu$ with an exponent $\nu = 3.3$.

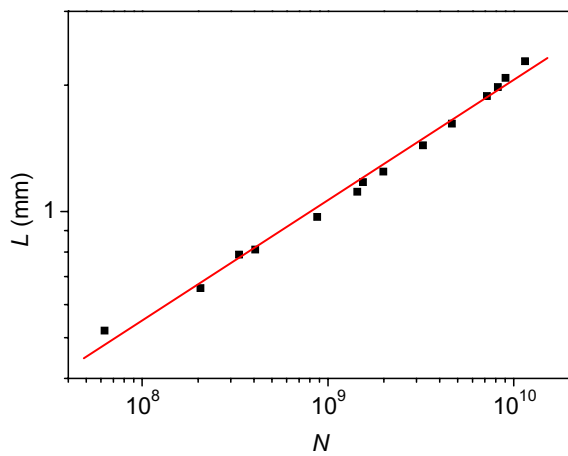


Figure 5. MOT size versus number of trapped atoms. The atom number is changed using the diameter of the repumper laser. The solid line (red online) shows that a single power law (exponent 0.29) fits the entire range of data.

The capture volume (V_{trap}) and the capture velocity (v_{capt}) depend on the size of the trapping and cooling lasers as well as on the size of the repumper laser. Changing the size Φ of any laser beam (cooling or repumper) is thus a very efficient way of controlling the number of atoms. In particular, one has $v_{\text{capt}} \propto \sqrt{\Phi}$ and $V_{\text{trap}} \propto \Phi^3$, which, using equation (15), yields $N \propto \Phi^4$. We can thus choose to control the number of atoms by changing the size of the repumping laser. As mentioned above, this allows one to change the number of atoms in the MOT while leaving the parameters of the incident laser beams, at the location of the MOT, unaffected. Figure 4 shows how the number of trapped atoms changes as we increase the size of the repumping laser beam (at standard MOT parameters). A slope of $N \propto \Phi^{3.3}$ is indicated in the solid line, close to the result obtained in [8].

3.2.2. MOT scaling law with $N(\Phi_{\text{rep}})$. Having validated our method to change the atom number via the size of the repumper laser, we used this procedure to study the scaling law of MOT size. Obviously, a systematic scan of all MOT parameters is far too complex, as there are too many parameters that have an impact on MOT size and density.

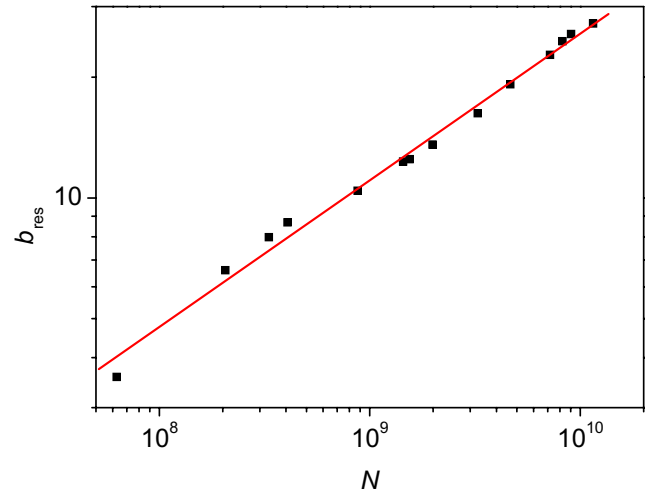


Figure 6. Optical thickness of the MOT versus number of trapped atoms. The atom number is changed using the diameter of the repumper laser. The solid line (red online) shows a power-law fit with an exponent of 0.37.

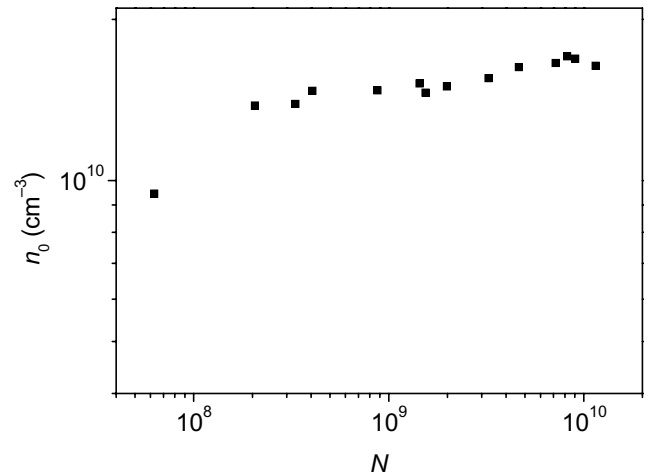


Figure 7. MOT peak density n_0 versus number of trapped atoms. The atom number is changed using the diameter of the repumper laser.

Thus, we choose to define a ‘standard’ set of parameters and investigate the MOT as we change one of the parameters, keeping the others fixed at the standard values as given in table 1. As shown in figure 5, we do observe a single scaling law up to $N = 10^{10}$. A power-law fit yields an exponent of $\alpha \approx 0.3$ scaling law close to $L(N) \propto N^{1/3}$. This is in excellent agreement with the standard Wieman model, but in contrast to the results observed previously in [4], where a strong deviation from $L(N) \propto N^{1/3}$ has been reported for an atom number larger than $N \approx 5 \times 10^7$. As we will show in the next section, this discrepancy has motivated us to perform further experimental studies with different protocols. But before turning to these different investigations, we want to point out that it is also possible to exploit the same experimental data to illustrate more efficiently the scaling law of the MOT. We obtain not only the size of the cloud, but also the resonant optical thickness b_{res} of the MOT (figure 6) and the behavior of the central density n_0 (figure 7) versus the number of atoms N . As described in section 2, the optical thickness b_{res} is extracted by using the signal at the center of

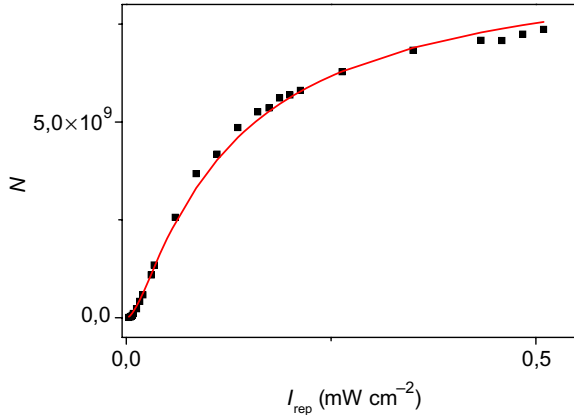


Figure 8. Experimental result for atom number as a function of repumper intensity. All other parameters correspond to the standard parameters, as defined in the text.

the fluorescence image, which is proportional to the integral of the atom along the line of sight, rescaled to the resonance $\delta = 0$. The peak density (n_0) extracted from the same data, assuming a Gaussian density profile, clearly indicates that we have a constant density of atoms up to $N = 10^{10}$.

The first conclusion of this study is that the Wieman model seems to apply even in our regime of a large MOT (containing up to 10^{10} atoms), which contradicts the earlier observation of [4]. We stress, however, that our conclusion is reached on the basis of the careful experimental procedure detailed in section 2, which differs from that used in previous studies.

4. Repumper intensity-controlled atom number: $N(I_{\text{rep}})$

Intrigued by the discrepancy mentioned above between the scaling we have obtained in the previous section and that observed by Sesko *et al* [4], we have investigated the role of the protocol used to modify the number of trapped atoms. Indeed, the number of atoms in a MOT depends on many control parameters, as indicated in table 1. In order to extend our studies of the MOT scaling laws, we have chosen another protocol to vary the number of trapped atoms in the experiment. The most convenient alternative method in our setup has been to modify the intensity of the repumping laser (I_{rep}). In practice, we change the power of the repumper laser, but as we keep the beam size constant in this run, this amounts to changing the repumper intensity. We note that in contrast to the previous method, using this protocol we also modify an external control parameter at the location of the MOT. As we will see, this will have an important impact on the scaling law of the MOT.

4.1. Experimental results on $N(I_{\text{rep}})$

4.1.1. Atom number versus repumper intensity: $N(I_{\text{rep}})$. Let us first discuss how the atom number is affected as we change the intensity of the repumper laser. Figure 8 illustrates how the number of atoms increases with the intensity of the repumper. A previous model [5] predicts the number of atoms growing as $N \propto v_{\text{capt}}^4$, where v_{capt} is the capture velocity of

the trap. The precise value of the capture velocity depends on parameters of the trapping and repumper lasers as well as on the magnetic field gradient. Within a simplified picture one can estimate the capture velocity from the laser-deceleration a and stopping distance of an atom, which needs to be smaller than the size of the laser beams L_{laser} , according to

$$v_{\text{capt}} \approx \sqrt{2apL_{\text{laser}}}. \quad (16)$$

Here we added a factor p as the trapping force is only effective for atoms in the bright state ($F = 3$) and the effective deceleration is roughly proportional to the bright-state population p . To determine its dependence on repumper intensity I_{rep} , we use simple rate equations and obtain

$$p = p_{\infty} \frac{I_{\text{rep}}}{I_p + I_{\text{rep}}}, \quad (17)$$

where p_{∞} denotes the bright-state population in the high-intensity limit. Equation (17) yields an approximate description for the population of trapped atoms, since both MOT and repumper laser parameters vary in space due to absorption inside the high-density atom cloud. According to the above argumentation, the number of trapped atoms is thus expected to scale as

$$N = N_{\infty} \left(\frac{I_{\text{rep}}}{I_N + I_{\text{rep}}} \right)^2, \quad (18)$$

where N_{∞} denotes the maximally trapped number of atoms. Even though this model seems very convincing, one should allow, in principle, that the parameters I_p and I_N could be different, as the hyperfine populations inside the MOT are not necessarily the same as in the loading region for the trap.

With these considerations, the atom number dependence of the repumper intensity and the bright-state population directly follows from equations (17) and (18):

$$I_{\text{rep}} = I_N \frac{N^{1/2}}{N_{\infty}^{1/2} - N^{1/2}}, \quad (19)$$

$$p = p_{\infty} \frac{N^{1/2}}{\beta N_{\infty}^{1/2} + (1 - \beta)N^{1/2}}, \quad (20)$$

where $\beta = I_p/I_N$. As demonstrated in figure 8, the derived atom number dependence on I_{rep} yields an excellent description of our experiment, with $N_{\infty} = 8.9 \times 10^9$ and $I_N = 0.05 \text{ mW cm}^{-2}$. Note that the precise value for these fitting parameters depends on various experimental conditions (such as power of the trapping and cooling laser) and can be different for the various experiments performed to extract the data shown in this paper. The loading efficiency, and consequently the number of trapped atoms, is determined by the population dynamics in a large volume around the trap, where we expect a good description by the above model. However, the measured bright-state population p mainly contains contributions from atoms confined in the MOT region, where level populations can be strongly altered by absorption of MOT and repumper lasers and by spontaneous Raman photons.

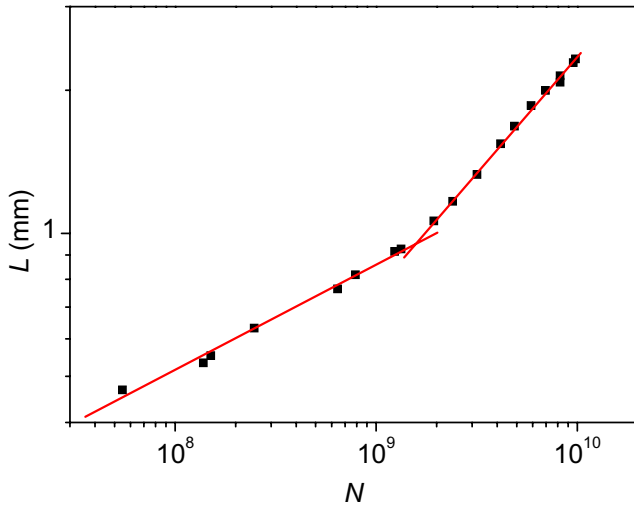


Figure 9. MOT size versus number of trapped atoms. The atom number is changed via the intensity of the repumper laser. The solid lines (red online) indicate the results of a fit, illustrating the different power laws below and above the threshold value ($N_{\text{th}} \approx 1.5 \times 10^9$).

4.1.2. MOT scaling law with $N(I_{\text{rep}})$. Having understood the dependence of atom number on repumper intensity, we can now study the scaling law of the MOT size $L(N)$, with $N(I_{\text{rep}})$ controlled via the repumping intensity. The resulting curve is shown in figure 9. Here again the repumper has been switched off after the MOT laser so that all atoms are pumped into the $F = 3$ hyperfine level before probing with a detuned laser (see appendix 7.1). One can clearly identify two regimes, separated by a threshold $N_{\text{th}} \approx 1.5 \times 10^9$. For $N < N_{\text{th}}$, we observe a scaling law close to that predicted by the Wieman model, while for $N > N_{\text{th}}$ the scaling law is nearly $L(N) \propto N^{1/2}$, which is also reminiscent of what has been observed previously [4]. However, these similarities are coincidental. Firstly, the procedures to vary N are different: in [4], N is tuned by acting on the loading of the trap without modifying the MOT control parameters, while in this part of our study we do vary one of the control parameters, namely the repumper intensity. Thus, it is the results obtained with our first procedure section 3.2.2 that should be compared with those of [4], and there we observe a single $N^{1/3}$ scaling law. Secondly, the measurement procedures are also different: our careful imaging procedure assures that we measure the actual atomic density profile, while the faster procedure of [4] (imaging of MOT fluorescence) does not offer this guarantee. A better understanding of MOT behavior might be obtained when looking differently at the same data, by extracting as in section 3.2.2 the on-resonance optical thickness b_{res} (figure 10) and the peak density n_0 (figure 11). These different ways of illustrating our experimental results reveal different phenomena. Figure 10, for instance, clearly shows that for $N > N_{\text{th}}$ the optical thickness b_{res} becomes roughly constant, which seems consistent with a scaling law of $L(N) \propto \sqrt{N}$. We also see that below the threshold value, the peak density of our cloud is not constant (figure 11), in contrast to what one might expect from the Wieman model. In this regime, $L(N)$ thus behaves differently from the scaling law $L(N) \propto N^{1/3}$. In the density plot, this difference is more pronounced than in the size plot.

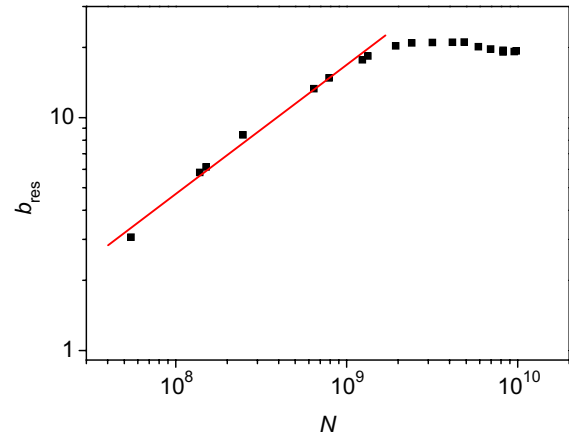


Figure 10. Optical thickness of the MOT versus number of trapped atoms. The atom number is changed via the intensity of the repumper laser. The solid line (red online) gives a power law with an exponent of 0.55 in the low atom number regime.

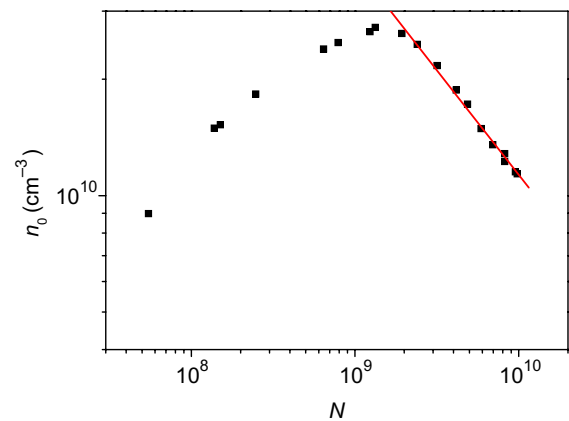


Figure 11. MOT peak density n_0 versus number of trapped atoms. The atom number is changed via the intensity of the repumper laser. The solid line (red online) is a power-law fit corresponding to $n_0 \propto N^{-0.54}$.

In order to quantify these two regimes, we have performed a systematic study of the scaling laws above and below the threshold value, extracting the power-law exponent $\alpha_{1/3}$ below the threshold and the exponent $\alpha_{1/2}$ above the threshold. The value of atom number N_{th} at the threshold and the size at threshold L_{th} are also given. All these results are summarized in table 2. The size scaling law for atom numbers below the threshold is different from the Wieman prediction ($\alpha_{1/3} = 1/3$) and has an exponent closer to ≈ 0.22 . For the scaling law above the threshold, we find values close to $\alpha_{1/2} = 0.5$. As we will see below, we do not have a complete explanation for the observed scaling law in all regimes. The data shown in this table might become useful once such a complete model has been developed.

One can note that the scaling law in the regime above the threshold value seems to be consistent with the observation of Lindquist *et al* [6] and with the conjecture $b(\delta) \approx 1$, arguing that the MOT will self-adjust to this value, beyond which multiple scattering becomes important [6]. As we will see in section 4.2, we derive this \sqrt{N} scaling law from completely different physical arguments, which are based on details of the trap loading as the repumping intensity is changed, and on the repartition of atoms among both hyperfine ground

Table 2. Systematic study of scaling law exponents and threshold value. We denote $\alpha_{1/3}$ as the exponent below and $\alpha_{1/2}$ as the one above the threshold N_{th} . The values indicated in this table have been extracted from a power-law fit. The standard parameters are given in the first line. The parameters that are changed are indicated in boldface. The repumper detuning is $\delta_{\text{rep}} = 0$ for all these experiments and the number of atoms has been changed via the intensity of the repumper.

δ_{MOT} (Γ)	I_{MOT} (mW cm^{-2})	∇B (G cm^{-1})	$\alpha_{1/3}$	$\alpha_{1/2}$	N_{th}	N_{max}	L_{th} (mm)
-2.5	7	10	0.22	0.49	1.6×10^9	9.8×10^9	0.96
-2	7	10	0.21	0.48	1.0×10^9	7.4×10^9	0.87
-3	7	10	0.24	0.45	1.6×10^9	9.0×10^9	1.01
-2.5	3.5	10	0.21	0.45	0.6×10^9	3.8×10^9	0.86
-2.5	1.75	10	0.23	0.41	0.16×10^9	0.38×10^9	1.15
-2.5	7	16	0.25	0.44	0.9×10^9	7.1×10^9	0.81
-2.5	7	5	0.20	0.43	0.47×10^9	1.9×10^9	0.96

states. Also, as we have seen in section 3.2.2, when the atom number is controlled using a different method, this \sqrt{N} scaling disappears, showing that the \sqrt{N} law is not a general feature for large traps.

In summary, the experimental results described in this section show the following:

- (i) We observe a scaling law $L(N) \propto \sqrt{N}$ above a threshold value N_{th} , when the atom number is changed via the intensity of the repumper.
- (ii) Below this threshold value, the density is not constant, in contrast to the Wieman model.

The different behavior observed with the two different methods used to control the number of atoms indicates the importance of the repumper laser. A model trying to explain the scaling law of MOT size in these regimes thus requires to go beyond a two-level model for the atoms, including, for instance, the internal degrees of freedom of the atoms.

4.2. Wieman–Pritchard model

The aforementioned Wieman model is based on a two-level model for the atom and, hence, neglects any effect of the repumper laser, which we expect to be important in the present case. Such multi-level effects have been previously considered, to reduce MOT laser rescattering and optimize atomic densities. Based on these concepts, Ketterle *et al* [12] have introduced the so-called dark SPOT. In such a trap, only atoms in the upper (‘bright’) hyperfine level are interacting with the cooling and trapping lasers, thereby reducing the light-induced atom–atom interactions. According to the model of [12], the balance between trapping, equation (11), and repulsion forces, equation (12) can be rewritten as

$$F_{\text{tr}} = -\kappa p r, \quad (21)$$

$$F_{\text{ms}} = G_3 p^2 n r. \quad (22)$$

Here $p = N_3/(N_3 + N_2)$ is the fraction of atoms in the bright hyperfine level. As only this part of the atoms interacts with the cooling and trapping lasers, the trapping force has to be multiplied by p . The repulsive interaction between atoms requires a pair of atoms in the bright state and one thus has to include a factor p^2 in F_{ms} . Consequently, the stationary atom density resulting from equations (21) and (22) has an additional p -dependence according to

$$n_{\text{WP}} = \frac{\kappa}{p G_3} = \frac{n_{\text{W}}}{p}. \quad (23)$$

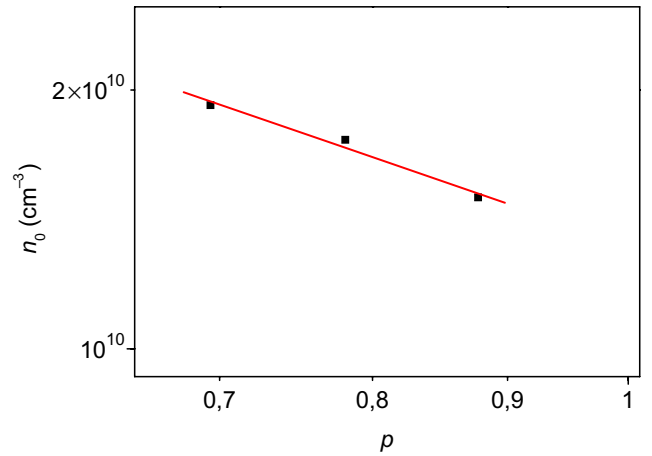


Figure 12. MOT peak density n_0 versus p . The solid line (red online) gives a power-law fit with an exponent of -1.05 , in agreement with the $1/p$ prediction of the Wieman–Pritchard model. The experimental data points correspond to the largest atom number obtained for $I_{\text{rep}} = I_{\text{rep}}^{\text{max}}/2$, $I_{\text{rep}}^{\text{max}}/4$ and $I_{\text{rep}}^{\text{max}}/10$ (corresponding to total atom numbers $N = 9.9 \times 10^9$, 7.8×10^9 , 4.7×10^9 and sizes $L = 2.1$, 1.8 , 1.5 mm respectively).

As this model is an extension of the one discussed in section 3.1, we call this the Wieman–Pritchard model.

In our experiments when we control the number of atoms by changing the intensity of the repumping laser, we clearly expect that the fraction p of atoms in the bright state is altered. Even though we do not use a dark region in our MOT, we realize what we call a self-adjusted dark MOT. One can now try to apply the Wieman–Pritchard model and investigate which scaling law would be predicted with the simplest ingredients. In figure 12, we plot the density at the MOT center versus the parameter p , obtained by detecting either only atoms in the $F = 3$ state (N_3) or all atoms ($N_2 + N_3$). The solid line is a power-law fit and gives an exponent of -1.05 , in agreement with the $1/p$ prediction of the Wieman–Pritchard model.

The Wieman–Pritchard model thus appears to explain our experimental results for large MOTs as the $L(N) \propto \sqrt{N}$ scaling law can be derived from this model. Indeed, as discussed in section 4.1.1, one expects both the atom number N and p to decrease as the intensity of the repumper is reduced. The bright-state fraction p approaches a constant value p_{∞} for large atom numbers but varies $\propto \sqrt{N}$ as the number of atoms is reduced (see equation (20)). Within the Wieman–Pritchard model, such a scaling law for

$p \propto \sqrt{N}$ predicts a density $n_{\text{WP}} \propto N^{-1/2}$ and thus a MOT size that scales as $L \propto N^{1/2}$. The Wieman–Pritchard model can thus explain our experimental observation in the large atom number regime. We want to stress again that a similar $L(N) \propto \sqrt{N}$ scaling law has been reported previously and attributed to higher-order MOT photon rescattering, without rigorous theoretical justification [6], while the $L(N) \propto \sqrt{N}$ scaling law presented in this paper can be explained without invoking higher scattering order, and depends on the method employed to change the number of atoms. Also, we recall that this power law disappears when the atom number is changed by varying the size of the repumping laser, keeping all the other parameters constant (see in figure 5), and this up to very large atom numbers ($N \approx 10^{10}$).

Despite the excellent agreement between the Wieman model and our experimental results of section 3 on one side, and the Wieman–Pritchard model and our results of section 4 for the large atom limit on the other side, there are some results that cannot be explained by the standard models used up to now for the MOT description. Indeed, one can see in figure 11 that for an atom number below $N = 10^9$, the density of atoms in the trap is neither constant (as predicted by a simple Wieman model) nor following the law deduced from the Wieman–Pritchard model (with $L \propto \sqrt{N}$). As we do not expect the trap nonlinearities nor the effect of nonuniform effective repulsion to play a role in these regimes, other complex mechanisms might be at work in these regimes. In [21], unusual hyperfine populations have been reported and an explanation based on a type of self-induced dark MOT model is suggested. A combination of the effects of such a self-induced dark MOT, resulting in modified hyperfine populations, together with the $L \propto \sqrt{N}$ scaling we observe when changing the atom number via the intensity of the repump laser might explain the results of previous experiments [6].

5. Beyond the standard models for MOT

5.1. Optical thickness of repumper and hyperfine pumping

A further observation shows another important aspect to be considered. As described in section 2, we use a repumper only along one axis (which is not along any axis of the MOT laser). It is thus possible to record the transmission of the repumping laser (even though without retro-reflection for this measurement). A screen placed on the repumper after it has passed the MOT allowed us to observe that the intensity of the repumper is considerably reduced by the MOT. This is a direct proof that the optical thickness for the repumper light is not small! Figure 13 shows an image of the repumper beam transmitted through the MOT. The dark region in the center indicates that many photons of the repumper are scattered by atoms of the MOT.

This qualitative observation has an important impact on the model we will use to describe the scaling law of MOT size. In that case, scattered repumping photons can be reabsorbed in the MOT, which will yield a repulsive force, in the same way as rescattered photons of the trapping light produce a repulsive force. Furthermore, the repulsive forces arising from rescattered repumping photons are not balanced

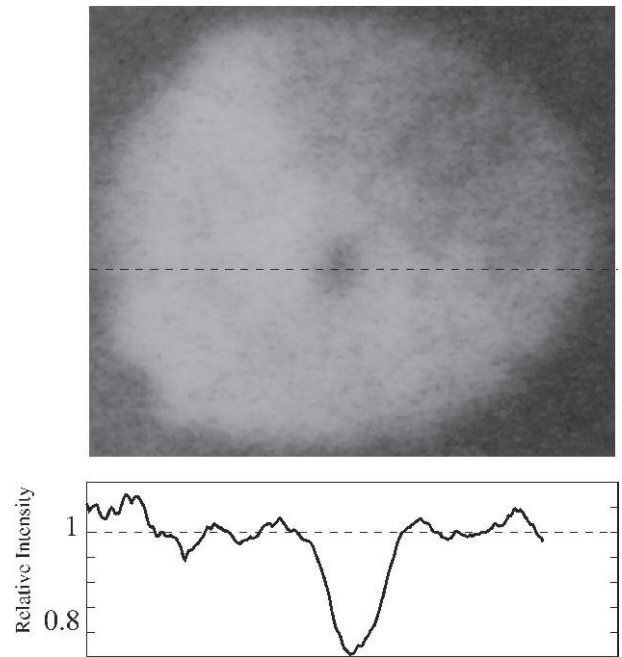


Figure 13. Image of transmitted repumper laser: the dark region in the center corresponds to the absorption of the repumper by MOT atoms in the dark state.

by any trapping or cooling force. In general, one has to analyze the subtle compensation between the repulsive forces due to rescattering and a shadow effect (resulting in a net compression along the axes of the laser) in order to know whether absorption and rescattering results in compression or repulsion. In our configuration, where the repumping laser is only present along one axis, the situation is somewhat different as there is no compression along the directions transverse to the repumper propagation axis.

We note that when we control the atom number via the size of the repumper laser, we cannot exclude the possibility that the average intensity of the trapping and/or repumping lasers is affected when the number of atoms is changed. Indeed, a modification in the optical thickness of the cloud may change the attenuation of the different incident laser beams as well as the importance of spontaneous Raman photons (resulting in a change of the hyperfine level), and thus affect the fraction of atoms in the bright state. To illustrate such effects, we have measured the number of atoms N_3 in the bright state $F = 3$ (no delay at repumper switch-off) and the total number of atoms $N_2 + N_3$ ($100 \mu\text{s}$ delay for repumper switch-off), in an experiment where the number of atoms has again been changed by varying the size of the repumping laser. In figure 14 we plot the proportion of atoms in the bright-state $p = N_3/(N_2 + N_3)$ as a function of the total number of atoms $N = N_2 + N_3$. As one can see, this proportion is roughly constant, except for low atom numbers, where it drops. This decrease of p is not understood, and the situation is far from trivial. The self-induced dark MOT proposed in [21] would predict a larger population of atoms in the dark state for larger atomic clouds, which is in contrast to our observation of figure 14. This decrease of p depends in a complex way on the relative attenuations of MOT and repumper lasers and on the presence of spontaneous Raman photons. A model to explain this decrease goes beyond a simple description using

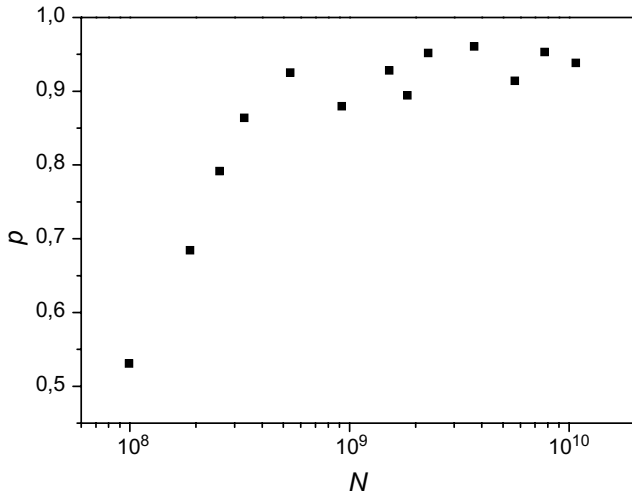


Figure 14. Proportion $p = N_3/(N_2 + N_3)$ of atoms in the bright ($F = 3$) state as a function of the total number $N = N_2 + N_3$. N is varied by changing repumper size.

low saturation and/or homogeneous laser intensities. From our experimental observation, we obtain a decrease of p for smaller atom number, whereas the density is roughly constant or slightly decreasing in this regime (see figure 7).

We have performed further experiments in order to investigate the role of the various parameters of the repumping laser. Changing the detuning of the repumper or its intensity did not dramatically alter the maximum density obtained in our trap. Even though we pass from a regime where the saturation of the repumping transition is larger than 1 to a regime where we do not saturate this optical transition, the relevant effective saturation to be considered is the efficiency of a repumping cycle versus the optical pumping into the $F = 2$ hyperfine level. Thus, one typically only needs 1 repumper photon for every 1000 photons exchanged on the main cooling and trapping transition. We thus estimate that the optical repumping cycle saturates 1000 times faster than the optical transition. Changing the detuning of the repumper from resonance to $\delta_{\text{rep}} = \pm 2\Gamma$ or $I_{\text{rep}}/I_{\text{sat}}$ from 1 to 0.1 does not drastically modify the repumping efficiency in our MOT. We have also verified that the size of the trap is the same if we detect atoms in both hyperfine levels or only in the bright state. This can be understood by the fact that atoms with a typical velocity of $v \approx 0.1 \text{ ms}^{-1}$ would have to spend a time of about $t \approx L/v \approx 10 \text{ ms}$ in the dark state, in order to undergo a larger spread than in the bright state [13]. This is not the case for our parameters. We also do not expect the trap nonlinearities or the effect of nonuniform effective repulsion to play a role in these regimes. We thus wonder whether new physical effects have to be added to explain the MOT behavior in these regimes.

5.2. Generalized Wieman–Pritchard model

In this section, we propose a new model that generalizes the existing theory by including the role of repumper photons. We note that this model is not valid for all MOT regimes. Indeed there are well-known regimes, which are not covered by the following discussion. The first one to mention is the temperature-limited regime, where MOT size is limited

by thermal atom motion and can be estimated from the equipartition theorem for the kinetic and potential energy of atoms in a damped harmonic trap. This regime is usually realized for very low atom numbers or when multiple scattering forces can be neglected, as e.g. in the case of narrow line cooling and trapping [22]. Other regimes at low or moderate atom number include situations where MOT size is so small that sub-Doppler cooling features have to be taken into account [23]. Further factors, such as free travel during a period in a dark state [13] or dynamical effects [18] (clearly becoming dominant when self-sustained oscillations set in [14]), can also affect the scaling law and the shape of MOTs with a large number of atoms.

The results of section 5.1 suggest that many repumper photons are absorbed by the atomic cloud, which may have a dramatic effect on MOT density. Similar to scattered MOT photons, scattered repumper light can be reabsorbed, which leads to an additional repulsive force between the atoms. On the other hand, as we do not use six counter-propagating laser beams for the repumper, the corresponding shadow effect for the repumper is negligible such that the net repulsion is important even for low values of the saturation parameter. As a rough estimate, we consider an optical thickness of $b_{\text{res}} = 40$ for the resonant $F = 3 \rightarrow F' = 4$ transition, with the repumping lasers being at resonance. The resulting repumper-optical thickness of the cloud for that frequency is of order $b_{\text{res}}(1-p)/p$. This means that even a 2% fraction of atoms in the ‘dark’ state yields an optically thick cloud for the repumping laser: $b_{\text{res}}(1-p)/p \approx 1$.

Accounting for the additional interactions, we thus propose the following generalization of the Wieman–Pritchard model by modifying the multiple scattering force:

$$F_{\text{ms}} = G_3 n p^2 r + G_2 n (1-p)^2 r, \quad (24)$$

where the parameter G_2 describes the repumper-induced interactions in analogy to G_3 for rescattered MOT photons. We will explicitly express in the following the dependence of G_2 on the intensity of the repumper and denote $G_2 = I_{\text{rep}} G_2^0$.

Again the stationary density is obtained from total force balance, which yields

$$\begin{aligned} n_{\text{WP+}} &= \frac{\kappa p}{G_3 p^2 + I_{\text{rep}} G_2^0 (1-p)^2} \\ &= \frac{n_{\text{W}}}{p + \alpha (I_{\text{rep}}/I_N) / (1-p)^2 / p}, \end{aligned} \quad (25)$$

where $\alpha = G_2^0 I_N / G_3$ describes the ratio between the interaction of atoms in the bright and the dark hyperfine level, at a reference intensity for the repumper of I_N . Note that both the bright-state population p and the atom number N depend on the repumper intensity I_{rep} . We can thus study the density $n_{\text{WP+}}$ as a function of p , I_{rep} or N . This equation predicts new scaling laws and new limits for the density of cold atomic clouds.

We stress that it is not straightforward to compare this model in a quantitative way to the experiments for several reasons. First of all, for large optical thickness of the repumper

and MOT lasers, the total number of atoms N and p become coupled parameters. Also, the effective local intensity to be considered for the interaction by the repumper laser depends on the optical thickness of the cloud. Furthermore, spontaneous Raman photons scattered on the $F' = 3 \rightarrow F = 3$ transition during a repumping process will be efficiently reabsorbed for a large optical thickness. Indeed, these photons are resonant with the $F = 3 \rightarrow F' = 3$ transition and the reabsorption of these photons corresponds to adding a depumping laser reducing the fraction p of atoms in the bright hyperfine level. These spontaneous Raman photons thus affect the bright-state population p but they will also contribute to a mechanical effect, as they are efficiently reabsorbed. Also, spontaneous Raman scattered photons (responsible for optical pumping from the $F = 3$ into the $F = 2$ hyperfine level and vice versa) can become important. For $N_{\text{at}} = 10^9$ atoms radiating every 10^3 absorption cycle a spontaneous Raman photon, we get a power of $P_{\text{Raman}}^{(1)} \approx 5 \mu\text{W}$ emerging from a surface of $L \approx 1$ mm. This corresponds to an intensity of $I_{\text{Raman}}^{(1)} \approx 0.5 \text{ mW cm}^{-2}$. However, these photons do not affect much atoms in the dark hyperfine level $F = 2$, as they are detuned by $\approx 20 \Gamma$ from the $F = 2 \rightarrow F' = 3$ transition. A direct and clean experimental study of these additional interaction effects would thus require a large detuning for the repumper (probably best done on the D1 line of Rb), so that the optical thickness of the repumper can be neglected and the new force can be eliminated. Such experiments go beyond the data we have gathered for this paper.

Let us consider the experiment where the atom number is changed via the intensity of the repumper and consider first a simple limit, i.e. without including the attenuation of the repumper beam. Even though this assumption is too crude for our experimental situation, this limit can illustrate some of the new features induced by taking into account the repulsion of the repumper photons. Assuming that p is a monotonous function of I_{rep} (see section 4.1.1), the Wieman–Pritchard model predicts an increase in the atomic density as I_{rep} is reduced and there is no maximum density until temperature effects set in. Equation (25), on the other hand, predicts a maximum in the atomic density when the term $\alpha(I_{\text{rep}}/I_N)(1-p)^2/p$ starts to dominate the first term in the denominator. The critical value of p and N , where this change appears, depends on the precise dependence of $p(I_{\text{rep}})$ and on the N dependence of I_{rep} itself. A quantitative description of our observations over the full range of experimentally realized atom numbers thus requires precise knowledge of the local repumper intensity and its effect on the bright-state population. As outlined above, a corresponding theoretical description turns out to be prohibitively complex, as attenuation and reabsorption lead to an intimate coupling between p and I_{rep} governed by the incident as well as the diffusive background of repumper photons, which all contribute to the repulsion forces and determine the value of p . Clearly, further experiments are required to uncover this complex interplay between the various atom–light and atom–atom interaction effects. Note that the attenuation of the repumper by cold atoms does not affect the dependence of $N(I_{\text{rep}})$ because the attenuation by the cold atomic cloud is only present at a small part of the capture volume for the MOT.

6. Conclusion

In summary, we have presented a systematic study of the various scaling laws appearing in large MOTs. In one series of experiments, where the atom number was changed by varying the diameter of the repumper laser, we recover the prediction of the Wieman model $L \propto N^{1/3}$, and thus a constant density, up to large atom numbers of $N \sim 10^{10}$, which provides strong evidence that an $N^{1/2}$ scaling law does not necessarily arise from multiple photon scattering as previously suggested in the literature. In another series of experiments, where we change the atom number via the intensity of the repumper laser, we found a cross-over in atom number dependence of MOT size changing from $L \propto N^{1/3}$ to $L \propto N^{1/2}$ with increasing N . We can explain the $L \propto N^{1/2}$ behavior using the Wieman–Pritchard model developed to describe a dark SPOT. We also point out unexplained behaviors that are observed in our experiment.

In addition, we suggest a new mechanical interaction effect induced by repumper photons, which can become important in large MOTs. Indeed, in certain regimes, in particular when more atoms are in the dark hyperfine state, repumper-induced interactions may impose an additional—previously overlooked—density limitation. A considerable density increase may hence be possible once these effects are understood in more detail. Further experiments are clearly required to investigate the role played by repumper photons on MOT density. One possibility, suggested by the model presented in this paper, is to use six independent repumper laser beams. The resulting shadow effect is expected to greatly compensate the repumper-induced repulsion between atoms, and consequently lead to denser atomic samples. A significant increase in atomic densities would be useful for the fast Bose–Einstein condensation of cold atoms and could possibly open the way to realizing Anderson localization of light with cold atoms, where very large spatial densities are required.

Acknowledgments

We acknowledge the financial support of CNRS, the PACA Region and ANR project CAROL (ANR-06-BLAN-0096). TP acknowledges support from the ESF program Quedis and from NSF through a grant for the Institute of Atomic, Molecular and Optical Physics (ITAMP).

Appendix A

A.1. Detuning the probe laser

In this appendix we describe some control experiments that we have performed in order to ensure that the size of the cloud of cold atoms we measure does not depend on the laser parameters used to probe the cloud. Multiple scattering is an obvious limitation for a precise measurement of the spatial size of the MOT. Even when the magnetic field gradient of the MOT is switched off, one would not expect to detect directly the fluorescence of atoms located on the opposite

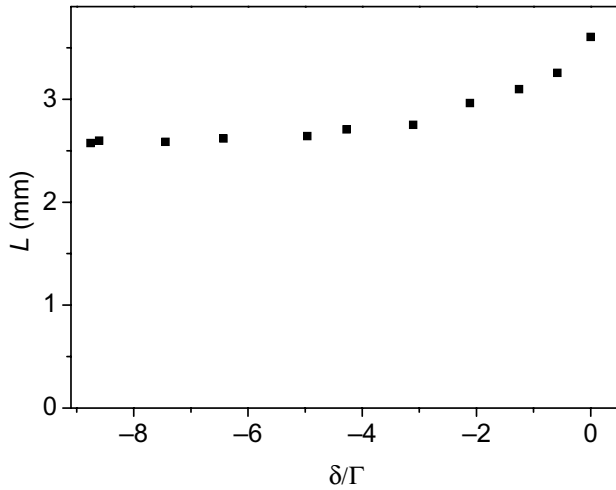


Figure A.1. Measurement of the apparent MOT size as a function of probe detuning for a MOT with our standard parameters, corresponding to a resonant optical thickness of $b_{\text{res}} = 40$.

side of the cloud when the photons scattered by these atoms cannot propagate directly to the CCD. Assuming e.g. that the apparent MOT profile would be described by $I(x, y) = n(x, y)(1 - b(x, y))$, where $n(x, y)$ is the real integrated density profile and $b(x, y)$ the optical thickness corresponding to that line of integration, one gets indeed a flattened apparent MOT profile for larger optical thickness.

This results in an apparent increase in the size of the cloud. A quantitative description of the dependence of the apparent MOT size as a function of probe detuning (not to mention any effect of magnetic field gradients) is very complex. But this effect can clearly contribute to a change of the apparent MOT size when the probe detuning is not large enough to avoid rescattering of light. In figure A.1 we show the experimental determination of the apparent MOT size as a function of the laser detuning used to probe the cold atomic cloud. One can see that for our MOT with a maximum optical thickness of $b_{\text{res}} = 40$, a probe detuning of $\delta = -6\Gamma$ is large enough to measure the real profile within satisfactory precision.

A.2. Time scales for hyperfine pumping

In our experimental setup, it is very convenient to delay or advance the cut-off of the repumper when we turn the MOT laser and magnetic field gradient off. Obviously, turning off the repumper much earlier than the MOT laser will empty the ‘bright’ ($F = 3$) state and put all atoms into the ‘dark’ state ($F = 2$). On the other hand, leaving on the repumper after turning off the MOT laser will repump all atoms into the $F = 3$ state. Probing the fluorescence with only the MOT laser turned on gives us a signal proportional to the number of atoms in $F = 3$. As shown in figure A.2, the time scale for repumping from $F = 2$ into $F = 3$ ($\tau_{\text{delay}} > 0$) is different from the time scale for pumping atoms into the ‘dark’ state $F = 2$ ($\tau_{\text{delay}} < 0$). The ratio N_2/N_3 of the number of atoms N_2 in the dark state and the number of atoms N_3 in the bright state can be extracted from the ratio of the pumping (Γ'_{pump})

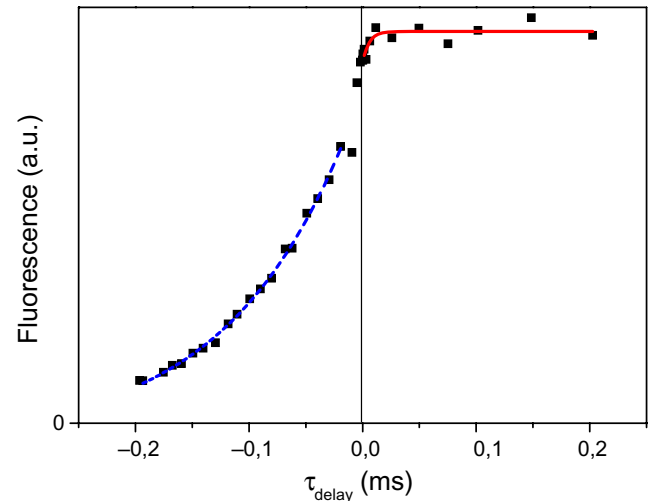


Figure A.2. Number of atoms in the bright state as a function of delayed repumper turn-off: τ_{delay} . The fit for $\tau_{\text{delay}} < 0$ (dashed line, blue online) gives a time scale of $110 \mu\text{s}$, whereas the fit for $\tau_{\text{delay}} > 0$ (solid line, red online) gives a time scale of $5.7 \mu\text{s}$.

and repumping rates (Γ'_{rep}):

$$\frac{N_2}{N_3} = \frac{\Gamma'_{\text{pump}}}{\Gamma'_{\text{rep}}}. \quad (\text{A.1})$$

From the fit of the experimental data, we extract a time scale for repumping of $\tau_{\text{rep}} = 1/\Gamma'_{\text{rep}} = 5.7 \mu\text{s}$ and a time scale for pumping into the dark state of $\tau_{\text{pump}} = 1/\Gamma'_{\text{pump}} = 110 \mu\text{s}$, predicting a ratio $N_2/N_3 \approx 0.052$. This is in rough agreement with the value obtained at zero delay ($\tau_{\text{delay}} = 0$): $N_2/(N_3 + N_2) \approx 0.076$. As expected, this shows that the repumping of atoms from $F = 2 \rightarrow F = 3$ is much faster than the optical hyperfine pumping from $F = 3 \rightarrow F = 2$.

References

- [1] Dalibard J and Cohen-Tannoudji C 1989 *J. Opt. Soc. Am. B* **6** 2023
- [2] Aspect A, Arimondo E, Kaiser R, Vansteenkiste N and Cohen-Tannoudji C 1988 *Phys. Rev. Lett.* **61** 826–9
- [3] Walker T, Sesko D and Wieman C 1990 *Phys. Rev. Lett.* **64** 408
- [4] Sesko D, Walker T and Wieman C 1991 *J. Opt. Soc. Am. B* **8** 946
- [5] Monroe C, Swann W, Robinson H and Wieman C 1990 *Phys. Rev. Lett.* **65** 1571
- [6] Lindquist K, Stephens M and Wieman C 1992 *Phys. Rev. A* **46** 4082
- [7] Steane A M, Chowdhury M and Foot C J 1992 *J. Opt. Soc. Am. B* **9** 2142
- [8] Gibble K E, Kasapi S and Chu S 1992 *Opt. Lett.* **17** 526
- [9] Petrich W, Anderson M H, Ensher J R and Cornell E 1994 *J. Opt. Soc. Am. B* **11** 1332
- [10] Townsend C G, Edwards N H, Cooper C J, Zetie K P, Foot C J, Steane A M, Szriftgiser P, Perrin H and Dalibard J 1995 *Phys. Rev. A* **52** 1423
- [11] Gabbanini C, Evangelista A, Gozzini S, Lucchesini A, Fioretti A, Müller J H, Colla M and Arimondo E 1997 *Europhys. Lett.* **37** 251–6
- [12] Ketterle W, Davis K B, Joffe M A, Martin A and Pritchard D E 1993 *Phys. Rev. Lett.* **70** 2253–6
- [13] Townsend C G, Edwards N H and Foot C J 1996 *Phys. Rev. A* **53** 1702

- [14] Labeyrie G, Michaud F and Kaiser R 2006 *Phys. Rev. Lett.* **96** 023003
- [15] Labeyrie G, de Tomasi F, Bernard J C, Müller C, Miniatura C and Kaiser R 1999 *Phys. Rev. Lett.* **83** 5266
- [16] Reinaudi G, Lahaye T, Wang Z and Guéry-Odelin D 2007 *Opt. Lett.* **32** 3143–5
- [17] Dalibard J 1988 *Opt. Commun.* **68** 203
- [18] Pohl T, Labeyrie G and Kaiser R 2006 *Phys. Rev. A* **74** 023409
- [19] Gattobigio G L, Michaud F, Labeyrie G, Pohl T and Kaiser R 2006 *AIP Conf. Proc.* **862** 211
- [20] Overstreet K, Zabawa P, Tallant J, Schwettmann A and Shaffer J 2005 *Opt. Express* **13** 9672
- [21] Muniz S, Magalhaes K, Henn E, Marcassa L and Bagnato V 2004 *Opt. Commun.* **235** 333
- [22] Chanelière T, He L, Kaiser R and Wilkowski D 2008 *Eur. Phys. J. D* **46** 507–15
- [23] Kim K, Noh H, Ha H and Jhe W 2004 *Phys. Rev. A* **69** 033406